# Detecting anomalies in diaphragm walls with electrical resistance measurements

Spruit, Rodriaan; van Tol, Frits; Broere, Wout; Slob, Evert

**DOI**
10.3997/1873-0604.2016022

**Publication date**
2016

**Document Version**
Final published version

**Published in**
Near Surface Geophysics

*Near Surface Geophysics, 2016,* **14**, 481-491 doi:10.3997/1873-0604.2016022

# Detecting anomalies in diaphragm walls with electrical resistance measurements

Rodriaan Spruit*, Frits van Tol, Wout Broere and Evert Slob

*Department of Civil Engineering, Delft University of Technology, the Netherlands*

Received August 2015, revision accepted June 2016

**ABSTRACT**

Quality control of diaphragm walls prior to excavation is often difficult. One technique that can be used to detect anomalies in diaphragm walls involves electrical resistance. Electrical resistance measurements across a diaphragm wall can (within a strict framework) be used to verify the presence of leaks in diaphragm walls as a supplement to crosshole sonic logging. From measurements around a test wall conducted in this study, it is concluded that the detectability of anomalies with electrical resistance decreases exponentially with the increasing distance between the measurement electrodes and the wall. Electrical resistance setups with two and four electrodes have been compared. For usable results, a four-electrode setup must be used in which the potential electrodes need to be placed very close to the wall (less than 0.2 m away). Based upon the test experience, a field setup for verification of a building pit consisting of diaphragm walls is suggested, as well as a setup for determining the quality of the concrete covering the rebar in quay walls constructed with diaphragm walls.

## INTRODUCTION

Diaphragm walls are frequently used for deep underground constructions in densely populated areas because of their high strength and stiffness in combination with quiet and vibrationless installation. Quality control for water tightness and retaining functions has been proved to be difficult as disasters during construction works in the Netherlands and Belgium have shown (Van Tol, Veenbergen, and Maertens 2010; Berkelaar 2011; Van Tol and Korff 2012). Other examples of underperformance have been reported in Boston (Poletto and Tamaro 2011), Cologne (Sieler *et al.* 2012), and Taipei (Hwang, Ishihara, and Lee 2007). The poor quality, or even absence, of concrete in the joints between the diaphragm wall panels is the primary cause of these calamities (Van Tol *et al.* 2010).

Because of these experiences, it was decided to investigate methods to detect anomalies in diaphragm walls, particularly around panel joints, prior to excavation of the building pit enclosed by the diaphragm walls. Although crosshole sonic logging (CSL) is the recommended method for detecting anomalies (Spruit *et al.* 2014), it is sometimes useful to be able to verify the outcome of such measurements with a physically independent measurement.

In Taipei, electrical resistance (ER) has been used successfully to detect anomalies in diaphragm walls (Hwang *et al.* 2007). However, in three field tests described in this paper and during metro construction works in Amsterdam (Van Tol *et al.* 2010), the interpretation of ER measurements showed low correlation with visually confirmed anomalies.

It was therefore decided to explore the limits of anomaly detection in diaphragm walls via a series of field tests on a concrete wall with known anomalies. In the tests, the electrode configuration has been varied, revealing a different detection limit for each configuration.

Based upon the results, electrode configurations for field tests will be recommended.

## MEASUREMENT PRINCIPLE

Electrical conductivity and/or resistance measurements are commonly used to detect leakage of membranes or sheet piled walls (Pellerin 2002). In the case of a plastic membrane, the contrast between the ER of a sound membrane and a leaking one is very high. During the measurement, electrical current is forced from one side of the barrier to the other using electrodes at a relatively large distance (approximately two times the investigation depth) from the

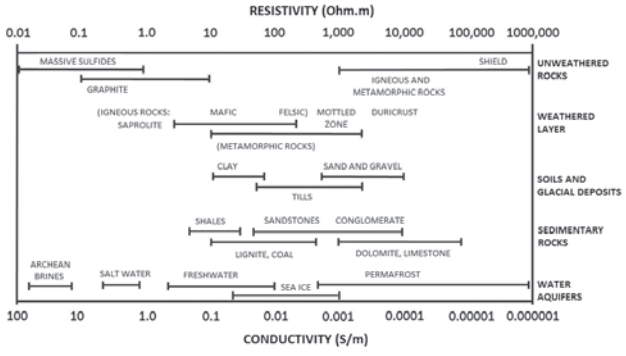


**Figure 1** Indication of resistivity properties (Gunn *et al.* 2014).

* r.spruit@rotterdam.nl

 

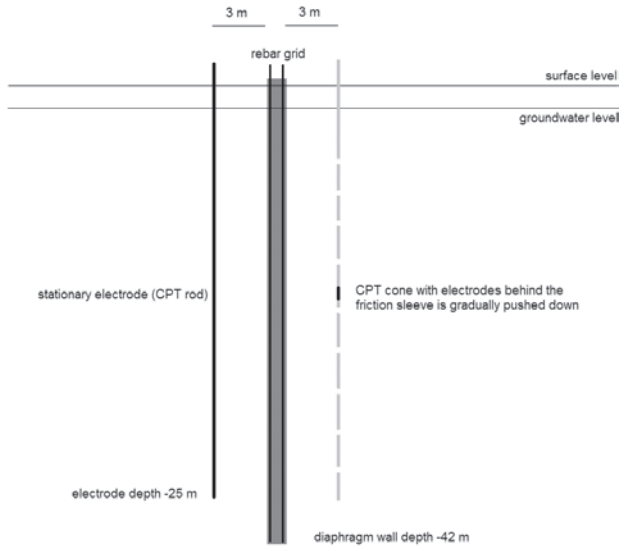


**Figure 2** Schematic cross section of the field test (not to scale).

**Figure 3** CPT truck during resistance measurements.

barrier. By measuring the local potential with separate electrodes, the resistance can be calculated from the potential difference and the input current, or the resistance can be determined directly by comparing the resistance with a calibrated resistor. With increasing potential electrode distance to the barrier, the resistance will be increasingly influenced by the larger volume of water. This will negatively affect the resolution of the measurements.

The ER method can be extended to tomography in which a large number of resistance measurements are taken with varying electrode configurations. By combining these measurements, it is possible to compute a 2D or 3D distribution of the resistivity (Pánek, Hradecký, and Šilhán 2008; Wilkinson *et al.* 2012). This principle is commonly used in geomorphology, archaeology, geohydrology, and ecology (Pánek *et al.* 2008; Ulrich, Günther, and Rücker 2008; Pellerin 2002). In such cases, a 3D model of the subsurface is the intended result of the measurements.

In the case of a diaphragm wall with defects, the position of the wall is known, and even the areas that are prone to show defects (the joints) are predefined. As a result, there is a much lower need for a full 3D model. Moreover, the use of a large number of electrodes, as is required for tomography, is not suitable to most building site conditions.

With a resistivity of up to 100 Ω·m (Neville 1981), saturated fully cured concrete has resistivity properties in the same range or just above clay and freshwater. Even if the defect affects the full cross section of the wall, the difference in resistance of an unaffected section of the wall and a section with a hole in it is relatively small. If the defect does not extend through the full cross section of the wall, the contrast in resistance will be even smaller. However, during construction of the Taipei metro (Hwang *et al.* 2007), ER measurements were used to locate leaks in diaphragm walls and to verify if the jet-grout repair works were successful. This indicates that ER is viable in detecting anomalies in diaphragm walls.

The aim of the tests is to find a straightforward measurement setup that involves a limited number of electrodes to limit time and space requirements in the field while still offering enough resolution to detect typical anomalies that can cause leaks in diaphragm walls.

## TESTS

### Field test

During the construction of the Kruisplein underground parking in Rotterdam in 2011, CSL and distributed temperature sensing (DTS) tests were executed on four joints to explore the possibilities of anomaly detection in diaphragm walls (Spruit *et al.* 2011). In joint 48-49, an anomaly in the CSL logs was found at 8.75 m below the top of the wall. Thus, this joint seemed suitable to test if the anomaly could also be found using an ER measurement. This was about one month after completion of the wall.

A day prior to the actual measurement, a stationary electrode was pushed in the soil on the outside of the building pit to a depth of 35 m below surface level, directly in front of the joint and 3 m away from the wall (electrode on the left in Figure 2).

On the test day, the cone penetration test (CPT) truck (Figure 3) was placed in front of joint 48–49 on the other side of the building pit (right side, Figure 2), 3 m away from the wall. The rebar cages on both sides of the joint and the previously placed stationary electrode were electrically connected to a switch box. This allowed the two electrode resistance measurement to be taken from the CPT cone to the electrode on the other side of the wall or from the CPT cone to the reinforcement cage north of the joint or from the CPT cone to the reinforcement cage south of the joint. Moreover, the local electrical ground resistance was measured in between two electrodes in the CPT cone. Each of these measurements was taken at 0.5-m interval. The cone, of which only one electrode was used for measuring the resistance to the stationary electrode and to the rebar cages, was a four-electrode GeoPoint earth resistivity cone.

The measurements were carried out using a two-electrode AC impedance tester Voltcraft LCR 4080, which operates at 120 Hz or 1 kHz. Using AC instead of DC avoids polarisation of the

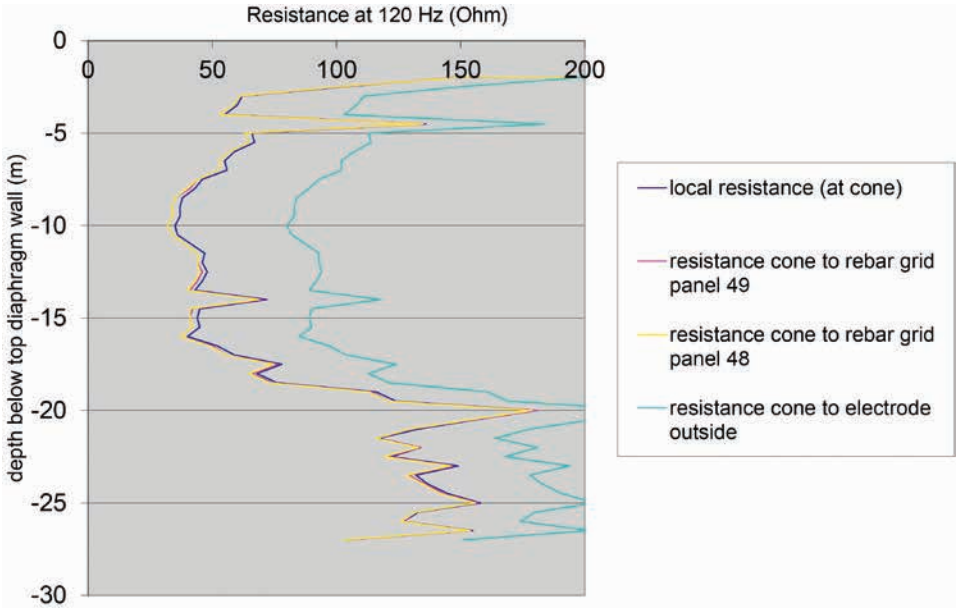


**Figure 4** Resistance at 120 Hz.

electrodes. In the two-electrode tests, the contact resistance causes a significant part of the measured resistance. The latter used four-electrode setup eliminates this contact resistance. The measurements show quite a lot of variation over the measured height, probably caused by variation in electrical properties of the soil, as indicated by the variation in the local resistance measured around the CPT cone.

Figure 4 shows the graphs of the local soil resistance (measured between two rings in the CPT cone), the resistance between the cone, and the rebar cages of both panels, and the resistance to the electrode on the opposite side of the diaphragm wall. All graphs run parallel to each other. In the upper five metres, high resistance has been recorded due to the partially saturated sandy top layer. Below -5 m, a sequence of clay and peat layers coincides with relatively low recorded resistance, with the peat layer between -8 and -10.5 m, showing the lowest resistance values. The very local higher resistance at -14 m corresponds with a 0.3-m-thick sand layer. This indicates that the contact resistance between the ring in the cone and the soil and/or the soil resistance may govern the measurements or that the defect in this specific joint does not extend to the full width of the diaphragm wall. Because of the strong effect of the thin sand layer, it appears that the measured resistance is primarily determined by the contact resistance of the electrodes in the CPT cone.

As a result, with a two-electrode setup, it will be hard to discriminate between defects in a diaphragm wall and soil resistivity variation or electrode contact resistance. For better results, a different electrode setup must be considered. It also seems worthwhile to use a reference measurement on an adjacent joint with no defects. The reference profile subtracted from the profile of the suspect joint might reveal the defects more clearly, assuming that the soil profile with its resistivity parameters is the same for both measurements.

**Figure 5** Test block subjected to ER measurement (dimensions: 1*2*2 $m^3$)

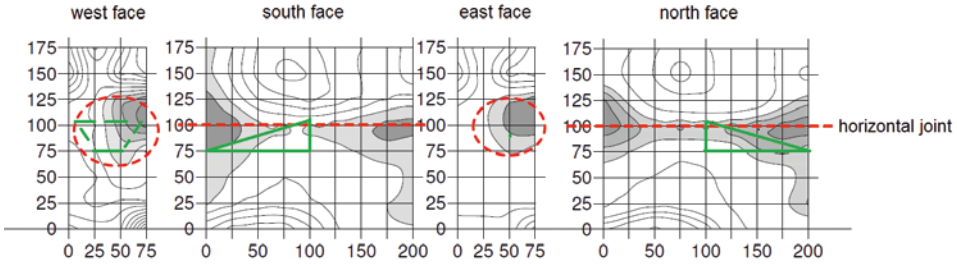


**Figure 6** Measurement results (dimensionless); dimensions in centimetres.

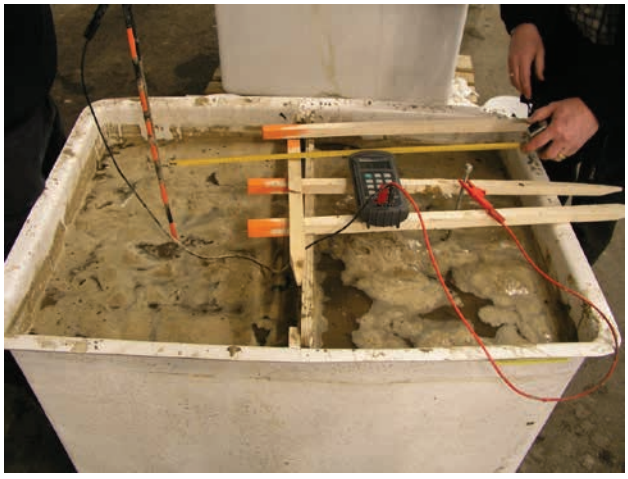

**Figure 7** Test container (dimensions: 0.9*0.5*0.5 $m^3$) with wooden barrier, water, and sand.

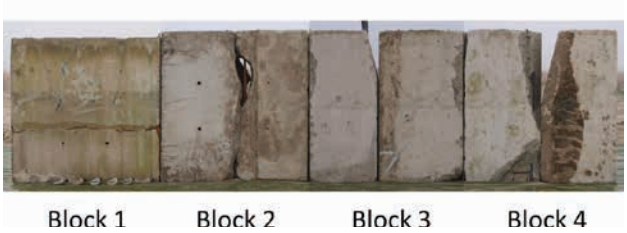


**Figure 8** Test wall (side view), dimensions: height=2 m, length=8 m, width=1 m.

### Tests on block with joint and anomaly

In 2011, a preliminary effort was conducted by a commercial company specialising in resistance measurements, using their detection method (Vanni and Geutebrück 2011) on one of the test blocks (Figure 5) that were produced for the CSL measurements (Spruit *et al.* 2014). This test block was submerged for two weeks in a large container filled with water, and on the day the tests took place, the block was removed from the container. During the test, 208 sensors were connected to the outer surface of the test block in a 0.25-m grid (Figure 6). Such a test setup cannot normally be realised with *in situ* D-walls.

The graphs provided by the company present a dimensionless parameter. Although the measurements theoretically contain resistance information, they are always reported as relative resistance. During the interpretation phase, the measurement results are scaled to such a degree that contrasts become visible in the graphs. The way this was done is not documented and depends on the engineer processing the data. Assuming that the dark areas indicate lower resistance (Figure 6), the joint between the two blocks could be located, but the included bentonite volume (indicated with green in Figure 6) could not.

The test does suggest that defects that continue throughout the total cross section of the concrete (in this case the joint between the two concrete blocks) might be located. However, the test block was saturated for two weeks and placed outside the water basin on the day of the tests. The concrete above and below the joint could have dried quicker than the concrete around the joint as the joint is partially filled with bentonite and will probably retain a higher moisture content because of this and the capillary effect of the joint.

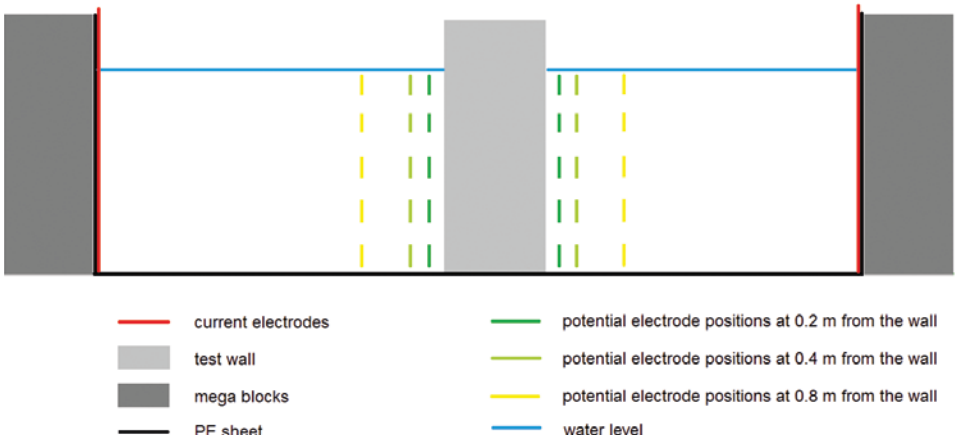


**Figure 9** Cross section of the test setup.

If in a real situation two joints would be compared, the joint with a higher hydraulic permeability is expected to show a lower ER compared with the better joint. If a comparative measurement setup between a known good joint and an uncertain joint is conducted, the scaling factors should remain the same for the reference and test joint.

**Tests in plastic container with wooden barrier**

Because of the unconvincing tests described above, the feasibility of resistance measurements was verified with a simple test.

A perforated wooden barrier was placed in the centre of a plastic container of 0.9*0.5*0.5 $m^3$ (Figure 7). The barrier was connected to the inside of the container using silicone. The perforations were detectable with a two-electrode AC impedance tester (Voltcraft LCR 4080) when the electrodes were close to the barrier. This indicated that a two-electrode setup could be feasible. However, the measurements showed a strong influence of the contact resistance between the electrode and the soil, possibly limiting the resolution of a two-electrode setup.

**Test wall in water basin**

Because of the previous test results, it was expected that only defects through the full cross section of the wall might be detected. The simple test in the container showed that the electrodes must be placed close to the object to make detection of defects possible.

From the two batches of test blocks intended for CSL measurements (see Spruit *et al.* 2014) (first set from 2010, second set from 2011), a total of four sets of two complementary blocks were available. To investigate the possibilities of electrical testing, the following test setup was prepared.

A continuous wall (Figure 8) containing all test blocks was built (eight sections, containing seven joints, of which four with defects and three with straight joints). This wall was placed into a basin containing water and/or soil.

The configuration with soil in the basin was discarded due to practical implications (water is easy to pump into and out of the basin, and varying the position of electrodes is easier). In most cases where leaks in diaphragm wall can cause problems, there will be a saturated sandy or gravelly soil; therefore, the electrical properties are governed by the electrical properties of the groundwater.

The installation of the experiment (Figure 9) consisted of the following steps:

- levelling and densifying the test area;
- spreading a 250-gr/$m^2$ polyethylene (PE) sheet;
- placing the test blocks on the PE sheet;
- folding the PE sheet inwards;
- placing the mega-blocks retaining wall elements around the test wall (see Figure 13);
- folding back the PE sheet, covering the floor and the inner vertical of the mega-block wall;
- filling the joints between the test wall and the PE sheet (floor and verticals adjacent to mega blocks) with polyurethane (PUR) foam;

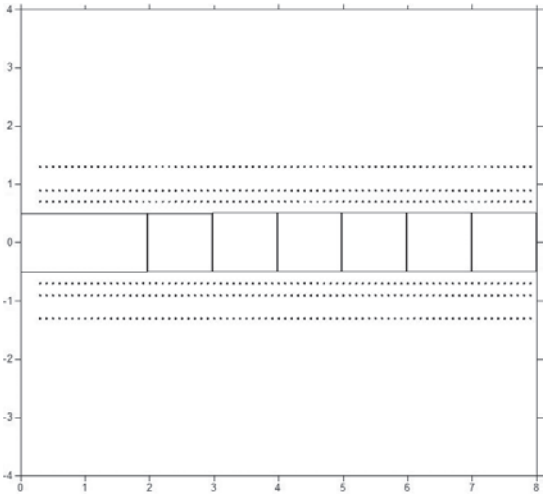


**Figure 11** Top view of test wall with electrode positions (dots) for measuring the potential at 0.2, 0.4, and 0.8 m distances to the test wall; horizontal dimensions (in metres).

**Figure 10** Top of test wall with track for positioning the potential electrodes.


**Figure 12** Current electrode grid.

- filling the three flat joints without defects with PUR foam;
- filling the basin with water from the nearby canal (conductivity = 134 mS/m, which is in the conductivity range of clays (Figure 1)).

The tests were intended to determine the maximum in situ distance between the electrodes and D-wall that would still offer a useful resolution for detecting defects. Due to geometric spreading of the potential around areas with high permeability, it was expected that when the electrodes were relatively far from the wall, only a blurred image could be obtained, whereas when "scanned" very close to the wall, even small defects might become visible.

It was therefore decided to test several distances between the wall and the potential electrodes, ranging from 0.2 m from the wall up to 0.8 m from the wall (see Figure 9). The current electrodes remained stationary during the tests.

The potential electrodes were installed onto a wooden frame bolted on a trolley. Both the horizontal distance of the potential electrodes to the wall and the vertical position of the potential electrodes (below the water level) could be adjusted. The trolley was able to run over a track that was installed on top of the test wall (Figure 10), providing the positioning of the electrodes parallel to the wall.

With the frame adjusted to the required electrode distances on both sides of the test wall and the depth below the water table, the trolley could be moved quickly (by means of a cable running through pulleys on both sides of the test wall) from one measurement position to the next (see Figure 11). The horizontal spacing of the potential electrode positions along the test wall was 0.1 m, resulting in 80 electrode positions along the wall at five different depths below the water table and at three potential electrode distances to the test wall (see Figures 9 and 11).

The test was carried out using a Gossen Geohm 2 earth resistance measurement device. The setup used four electrodes: two current (stationary) and two potential (varying position) (see Figures 9 and 11). The Geohm 2 measures resistance directly by means of comparing the actual resistance with a calibrated internal resistor. By turning the variable resistor until no current is running through the bridge circuit, the resistance can be read directly from the variable resistor dial. The injected current is emitted at 108 Hz.

**Figure 13** Test setup overview (looking northeast).

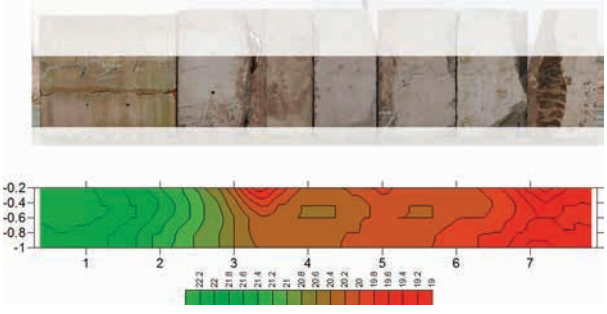


**Figure 14** Resistance (in ohms) results for potential electrodes, 0.2-m distance to the test wall (*x*-axis and *y*-axis in metres).

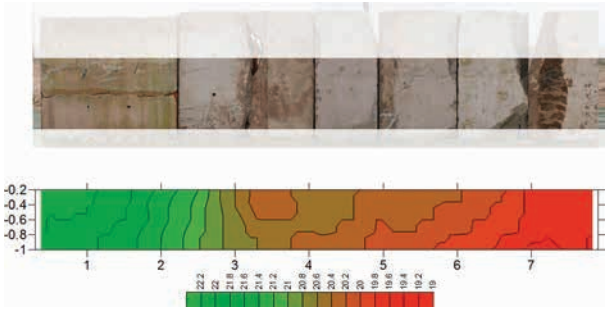


**Figure 15** Resistance (in ohms) results for potential electrodes, 0.4-m distance to the test wall (*x*-axis and *y*-axis in metres).

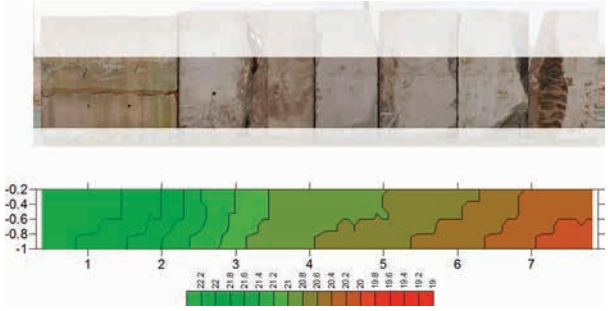


**Figure 16** Resistance (in ohms) results for potential electrodes, 0.8 m distance to the test wall (*x*-axis and *y*-axis in metres).

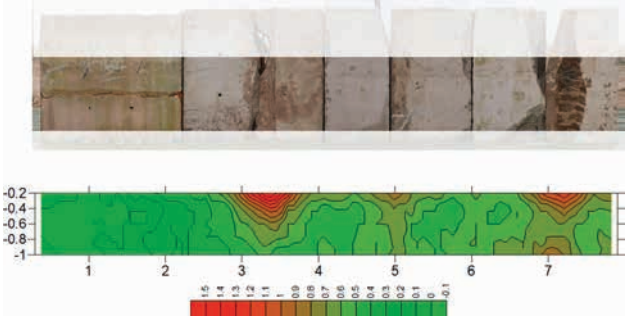


**Figure 17** Resistance (in ohms) results for potential electrodes, 0.2-m distance to the test wall, corrected with the results at 0.8- m distance (*x*-axis and *y*-axis in metres).

| Electrode distance to object (m) | Detection limit illustrated | Description of known anomaly | Anomaly size ($m^2$) |
|---|---|---|---|
| 0.1 | Figure 18 at 5.0 m | Cast concrete joint of 1 mm wide and 0,1 m high | 0.0001 (0.1 m * 0.001 m) |
| 0.2 | Figure 14 At x=5.0 m Y=-0.2 m | Opening of 2 cm by 5 cm | 0.001 (0.02 m * 0.05 m) |
| 0.4 | Figure 15 At x=3.5 m Y=-0.4 m | Opening of 10 cm by 20 cm | 0.02 (0.1 m * 0.2 m) |
| 0.8 | No anomalies detected | N/A | N/A |

**Table 1** Detected anomaly size.

The horizontal spacing of the measurement points was 0.1 m, and the vertical spacing is 0.2 m, which was also the exposed electrode length. The potential electrodes consisted of 1.5-mm-diameter copper wire installed vertically on a wooden frame.

The dots presented in Figure 11 only show the horizontal distribution of the measurement locations. During the tests, five depths were measured, i.e., at 0.2, 0.4, 0.6, 0.8, and 1 m below the water table.

The current electrodes were galvanised iron grids (Figure 12) fully covering the outer walls parallel to the test wall (Figure 9). This ensured current lines perpendicular to the test wall in case of a homogeneous resistivity of the test object.

Figures 14, 15, and 16 show the resistance results for the electrode distance to the test wall of 0.2, 0.4, and 0.8 m, respectively.

When the electrodes are located at 0.2 m to the test wall (Figure 14), the defects at 3.2, 5, and 7 m are recognisable by the relatively low resistance.

Block 1 does not show a defect, although a known bentonite inclusion is inside. Moreover, the horizontal joint at half height does not show up in the measured resistance. The joints that were injected with PUR foam (at 0, 2, 4, 6, and 8 m) are invisible in the resistance measurements. This indicates that it is likely that only defects extending the full width of the wall can be detected with these ER measurements. This seems to be coherent with the measurements described in Section 2.

After increasing the distance of the electrodes to the test wall from 0.2 to 0.4 m (Figure 15), most details are already lost. The only defect that is still recognisable is at 3.2 m. The average resistance has not changed much, suggesting that the resistance is mainly governed by the properties of the wall and that the additional water between the electrodes has a negligible effect on the absolute value of the measurements.

After increasing the distance between the electrodes and the wall from 0.4 to 0.8 m (Figure 16), there are no longer any recognisable defects. The average resistance along the wall is still in the same league as during the tests with the electrodes closer to the test wall, confirming that the resistivity of the test wall is the predominant factor in this test.

A trend with high resistance on the left and low resistance on the right can be recognised in Figures 14–16. By subtracting

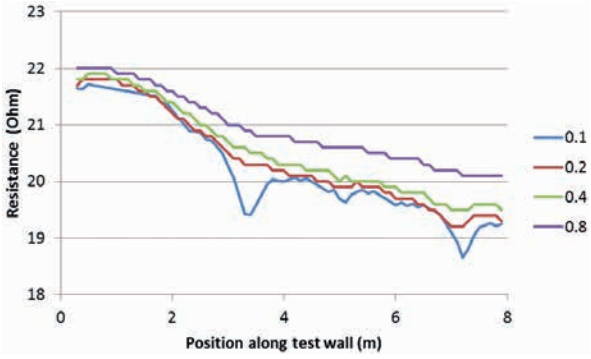


**Figure 18** Resistance at 1 m below water table for 0.1, 0.2, 0.4, and 0.8-m electrode distance to the test wall.

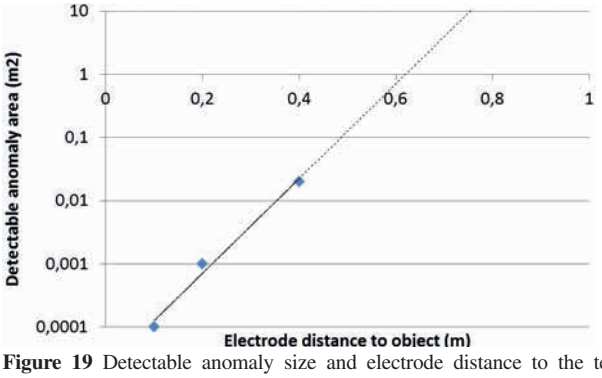


**Figure 19** Detectable anomaly size and electrode distance to the test object.

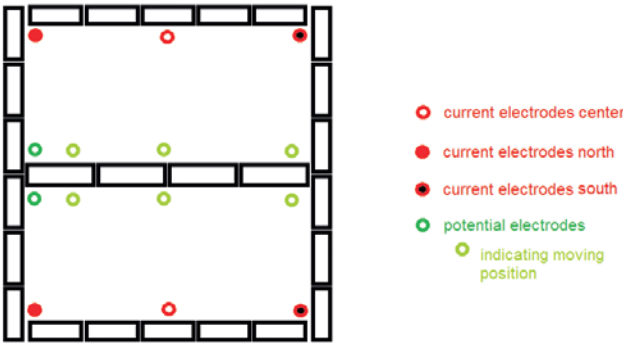


**Figure 20** Current electrode positions for single rod electrodes.

the resistance results at 0.8 m between the test wall and potential electrodes from the results at 0.2 m, this trend is effectively filtered out, as shown in Figure 17. Even the joints at 5 and 6 m, which were not distinguishable before, show up.

An extra run at one depth with 0.1-m separation from the wall was made (see Figure 18), although such a small distance increases the practical problems with irregularities on the outside of the D-wall. Moreover, push-in electrodes tend to deviate towards areas with lower horizontal stresses (due to the excavation of the D-wall trench), probably resulting in push-in electrodes hitting the concrete of the D-wall more often if introduced this close to the wall.

If the scan line at 1-m water depth is plotted for all electrode distances to the test wall (including the extra scan line at 0.1-m distance between the potential electrodes and the test wall) (see Figure 18), it becomes clear that the resolution for local anomalies dramatically decreases with increasing distance of the electrodes to the test object.

Based on the average size of the anomalies and the limits of detection, an estimated detectable anomaly as a function of electrode distance to the object has been constructed. Table 1 shows an overview of the typical anomalies that were detectable at the different electrode distances to the test wall.

When the above results are plotted on a logarithmic scale for the anomaly area (Figure 19), it becomes clear that, at 0.8-m electrode distance to the object, no anomalies were found because all anomalies in the test wall were smaller than 10 $m^2$.

Because the described electrode grids cannot be used in situ, the influence of the shape of the current electrodes on the resistance results has been investigated.

Instead of grids covering the full side of the basin, single vertical steel rods in the middle and corners of the outer walls of

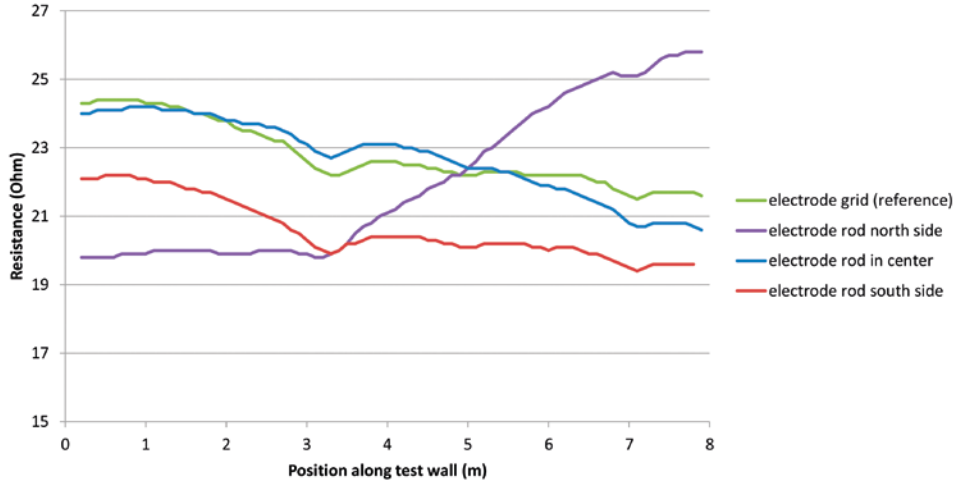


**Figure 21** Current electrode shape and position influence (position 0 is north side of test wall).

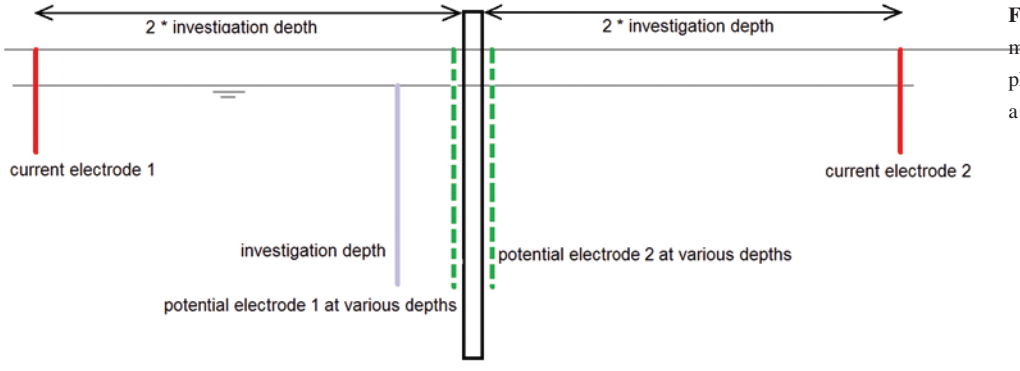


**Figure 22** Suggested measurement setup for testing a diaphragm wall before excavation of a building pit (side view).

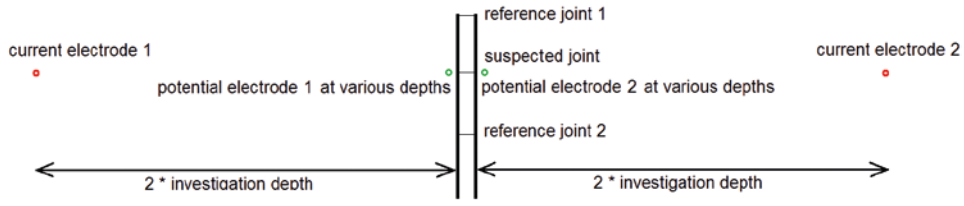


**Figure 23** Suggested measurement setup for testing a diaphragm wall before excavation of a building pit (top view).

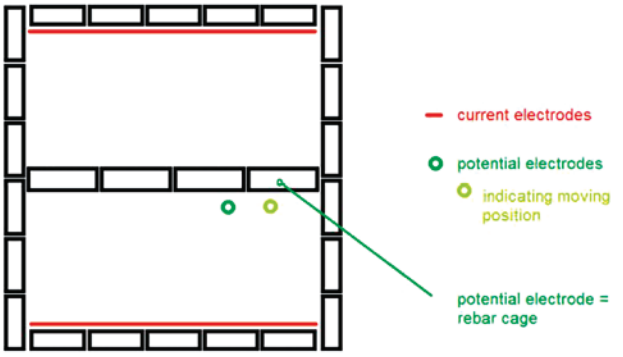


**Figure 24** Test setup with two current electrodes, one mobile potential electrode, and the rebar cage acting as the second potential electrode (four-electrode setup).

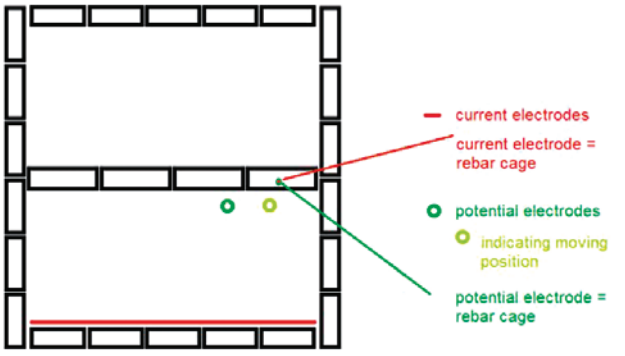


**Figure 26** Test setup with one distant current electrode, one mobile potential electrode, and the rebar cage acting as both the second potential and the second current electrode (three-electrode setup).

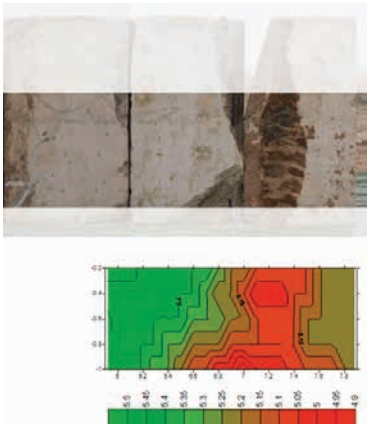

**Figure 25** Resistance (in ohms) results for the four-electrode test setup as indicated in Figure 24 (x and y axes in metres).

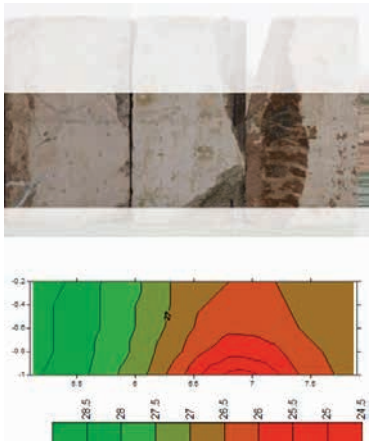

**Figure 27** Resistance (in ohms) results for the three-electrode test setup as indicated in Figure 26 (*x*-axis and *y*-axis in metres).

the basin were used as current injection electrodes (Figure 20).

Figure 21 shows the difference in measured resistance between the grid-shaped current electrodes and the single vertical steel rods in the outer corners of the test basin (north and south) or in the centre of the outer walls (see Figure 20 for electrode positions).

The resistance is influenced by the position and the shape of the current electrodes. The electrodes in the outer corners of the basin show a large deviation from the measurements with the electrode grids. This is probably caused by the asymmetric distribution of the current and potential lines due to the isolated walls of the basin. The image obtained with the electrodes in the centre of the outer walls is rather useable. The difference between the grid electrodes and the single rods in the centre of the outer walls of the test setup is almost negligible. In a field setup, single electrodes may therefore be used as long as the target area is more or less in the middle of the shortest line between the current electrodes.

*Suggested measurement setup*

From the measurements, it can be concluded that a successful setup should include the following components:

- A four-electrode setup in which a current is fed from current electrode 1 to current electrode 2, across the wall. The local potential at close distance to the wall is measured with potential electrodes 1 and 2, running simultaneously vertically along the joint(s) (Figures 22 and 23). It will already be hard enough to detect anomalies; contamination from electrode–soil contact resistance is unavoidable with a two-electrode setup. The contact resistance will probably obscure the small effect of an anomaly. With a four-electrode setup, the influence of contact resistance is negligible.
- Perform a relative measurement using known good joints as references (from CSL measurements).
- Current electrodes should be placed at least 3 m into the groundwater to guarantee good contact.
- Current electrodes should preferably be placed more than two times the investigation depth away from the wall that is being tested.
- Potential electrodes should be located less than 0.2 m from the wall.

The image can be improved by subtracting an average resistance image, taken farther away from the test object (e.g.,

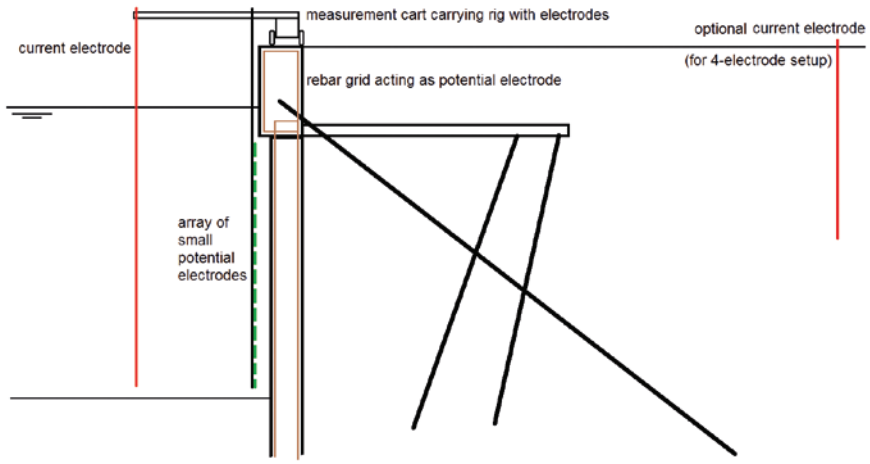


**Figure 28** Suggested three-electrode measurement setup (with an optional fourth electrode) for concrete quality check on quay walls.

0.8 m), from the resistance image recorded at short distance to the test object.

**Test wall in water basin, tests intended for diaphragm wall as quay wall (water on one side)**

Recent inspections of quay walls with diaphragm walls as retaining structures in the harbour of Rotterdam have shown areas coloured by iron oxide. This could indicate that there is local insufficient quality of the concrete cover, allowing the rebar cage to corrode. Incidentally, due to transport, some of the test blocks had chipped corners, exposing the rebar. This allowed for the field test to be extended to checking the feasibility of an alternative measurement technique for concrete cover quality. To this end, tests were executed with one of the electrodes connected to the exposed rebar grid in the test block.

Two setups were used:

- current electrodes as before (iron grids parallel to the test wall), with one of the potential electrodes connected to the rebar grid (four-electrode setup, Figure 24);
- one current electrode connected to the rebar grid, also acting as a potential electrode (three-electrode setup, Figure 26).

When Figure 25 is compared with Figure 27, the four-electrode setup (Figure 25) clearly shows a more detailed image of the exposed rebar cage. A four-electrode setup is much more cumbersome in the field because the current electrode on the land side cannot be easily moved. As the three-electrode setup also provides a rough identification of the exposed rebar area, a phased field survey could be effective.

First a three-electrode setup survey can be executed to quickly discriminate between good and inferior sections. The inferior sections can be further investigated using a four-electrode setup.

It will be necessary to use cores to calibrate the actual concrete quality and thickness of the concrete covering the rebar cage with the resistance results as these will depend on the local resistivity of the water and concrete mixture.

From the above results, the measurement principle illustrated in Figure 28 (without the optional current electrode on the land side) is suggested for large-scale testing of the quality of diaphragm wall concrete. If anomalies are detected, a local four-electrode measurement setup, illustrated in Figure 28 with the optional current electrode, can be used to better determine the size and shape of the anomaly. Note that such a measurement setup has not been tested within the scope of this research. Based upon the results of the test, it is expected that damaged or low-grade concrete covering the rebar cages can be detected using the above-described procedure.

## CONCLUSIONS AND RECOMMENDATIONS

In this study, a test wall with known anomalies has been used to determine the detectability of the anomalies with ER measurements. The tests described in this paper were conducted in water without the soil that would normally be present since, in permeable layers, where leakage may be a problem, the resistance is governed by the resistivity properties of the groundwater. As such, the results of these tests are expected to be applicable to permeable soil conditions.

ER measurements can be used to locate defects that extend to the full thickness of a diaphragm wall if the following requirements are met:

- A four-electrode measurement setup is used.
- The potential electrodes are placed very close to the wall that is being examined (potential electrodes more than 0.2 m away from the wall already seems to render the measurement useless).
- A reference measurement on a known good diaphragm wall joint at close distance (with the same geological profile) should be used to reliably identify anomalies.

Because of the limited reliability of the resistance measurements in this application, they should always be considered a verification option: The primary detection of anomalies in diaphragm walls should preferably be based upon CSL. As the resistance measurements seem to only be capable of locating defects that affect the full cross section, the ER method could be used to assess the risk of leakage, provided that CSL measurements have already identified anomalies. Installing the electrodes at less than

0.2 m from the wall can best be based upon the use of perforated standpipes, installed in boreholes. Push-in electrodes will have a higher chance of hitting the wall during installation if introduced at such short distance.

Attention should be paid to:

- the effect of clay/soil/bentonite in the defect on the resistance measurements;
- the effect of varying soil properties on the resistance results;
- the cost and reliability of the ER survey in comparison with the cost and reliability of repairing the wall with jet grouting. For some projects, pre-emptive repairs of anomalies will be more cost effective than reassessment of the anomaly with resistance measurements.

If a diaphragm wall is already exposed on one side, for example, if the building pit has been excavated in submerged conditions or if a harbour along a quay wall has been dredged, the quality of the concrete covering the rebar cages can be verified with ER if:

- a galvanic connection with the rebar cages can be made;
- calibration cores are available;
- there is water on the exposed side of the wall.

For a quick scan, a three-electrode measurement setup can be used, which can be further improved to a four-electrode setup if anomalies are detected. The four-electrode setup requires an extra current electrode in the soil on the land side of the wall, making the measurement more time-consuming and cumbersome, but delivering a much more detailed image of the quality variation of the concrete covering the rebar cages.

Electrical measurements in a four-electrode setup are capable of locating anomalies in diaphragm walls but they are not expected to find any anomaly in case the potential electrodes are placed farther away than 0.2 m from the test object.

## ACKNOWLEDGEMENTS

This research was funded by the Dutch research program "GeoImpuls."

## REFERENCES

Berkelaar R. 2011. Risk management during the reconstruction of the underground metrostation Rotterdam Central Station. In: *Proceedings of the Third International Symposium on Geotechnical Safety and Risk* (eds. N. Vogt, B. Schuppener, D. Straub and G. Bräu), pp. 643–650.

Gunn D.A., Chambers J.E., Uhlemann S., Wilkinson P.B., Meldrum P.I., Dijkstra T.A. *et al.* 2014. Moisture monitoring in clay embankments using electrical resistivity tomography *Construction and Building Materials* **92**, 82–94.

Hwang R.N., Ishihara K. and Lee W.F. 2007. Forensic studies for failure in construction of an underground station of the Kaohsiung MRT system, pp. 144–148. In: *Proceedings of Forensic Geotechnical Engineering* October 2009. International Society for Soil Mechanics and Geotechnical Engineering TC 40.

Neville A.M. 1981. *Properties of Concrete*, *2nd edn*. Longman Scientific & Technical Publisher.

Pánek T., Hradecký J. and Šilhán K. 2008. Application of electrical resistivity tomography (ERT) in the study of various types of slope deformations in anisotropic bedrock: case studies from the Flysch Carpathians. *Studia Geomorphologica Carpatho-Balcanica* **42**, 57–73.

Pellerin L. 2002. Applications of electrical and electromagnetic methods for environmental and geotechnical investigations. *Surveys in Geophysics* **23**, 101–132.

Poletto R.J. and Tamaro G.J. 2011. Repairs of diaphragm walls, lessons learned. In: *Proceedings of the 36th Annual Conference on Deep Foundations, Boston MA, USA*.

Sieler U., Pabst R., Neweling G. and Moormann C. 2013. Der Einsturz des Stadtarchivs in Köln: Bauliche Maßnahmen zur Bergung der Archivalien und zur Erkundung der Schadensursache. *BauPortal* **1**, 2–7.

Spruit R., van Tol A.F., Hopman V. and Broere W. 2011. Detecting defects in diaphragm walls prior to excavation. In: *8th International Symposium on Field Measurements in GeoMechanics (FMGM2011)*.

Spruit R., van Tol A.F., Broere W., Slob E. and Niederleithinger E. 2014. Detection of anomalies in diaphragm walls with crosshole sonic logging. *Canadian Geotechnical Journal* **51**, 369–380.

Ulrich B., Günther T. and Rücker C. 2008. Electrical resistivity tomography methods for archaeological prospection, layers of perception. In: *Proceedings of the 35th International Conference on Computer Applications and Quantitative Methods in Archaeology (CAA), Berlin, Germany, April 2–6, 2007*.

van Tol A.F., Veenbergen V. and Maertens J. 2010. Diaphragm walls, a reliable solution for deep excavations in urban areas? In: *DFI and EFFC, London: Deep Foundation Institute*, pp. 335–342.

van Tol A.F. and Korff M. 2012. Deep excavations for Amsterdam metro North–South line: An update and lessons learned. In: *Geotechnical Aspects of Underground Construction in Soft Ground – Proceedings of the 7th International Symposium on Geotechnical Aspects of Underground Construction in Soft Ground*, pp. 37–45.

Vanni D. and Geutebrück E. 2011. Leak detection in complex underground structures using an innovative geophysical method. In: *Proceedings of the Seventh International Symposium on Geotechnical Aspects of Underground Construction in Soft Ground, Rome, Italy, 16-18 May 2011* (ed G. Viggiani). Taylor & Francis Group, London, U.K.

Wilkinson P.B., Loke M.H., Meldrum P.I., Chambers J.E., Kuras O., Gunn D.A. *et al.* 2012. Practical aspects of applied optimised survey design for electrical resistivity tomography. *Geophysical Journal International* **189**, 428–440.